Updating of a deterministic model for the free thermal strain of concrete in fire during heating and cooling using novel experimental data and Bayesian inference

Florian Put[a*], Roberto Felicetti[b], Andrea Lucherini[c], Bart Merci[a], Ruben Van Coile[a]

[a] Department of Structural Engineering and Building Materials, Ghent University, Technologiepark-Zwijnaarde 60, Gent, Belgium, Florian.Put@UGent.be

[b] Dipartimento die Ingegneria Civile e Ambientale, Politecnico di Milano, Italy.

[c] Department for Fire-Safe Sustainable Environment (FRISSBE), Slovenian National Building and Civil Engineering Institute (ZAG), Slovenia.

*Corresponding author

Abstract

With the rise of performance-based structural fire design, understanding the behaviour of materials during both the heating and cooling phases of a fire has become essential. Traditionally, research has focused on the heating phase, resulting in limited data on material properties during cooling, in particular for the free thermal strain of concrete. This gap is critical, as free thermal strain significantly influences load redistribution in reinforced concrete structures. Two experimental campaigns were conducted to expand the available data: one using the UGent HIFREP ('High Intensity Fast-Response Electric Radiant Panel') and the other employing an electric furnace. The first test campaign provided an extensive dataset on the residual thermal strain, whereas the time-consuming furnace tests provided data for the entire fire event (heating and cooling). These datasets were used to update an existing model through Bayesian inference, coherently integrating the new information. The outcome is a comprehensive probabilistic model that accurately captures the free thermal strain behaviour of concrete throughout both heating and cooling, allowing for a full reliability-based evaluation of concrete structures in fire.

Keywords: concrete; cooling; free thermal strain; fire safety; structural fire engineering; experiments; Bayesian inference

Highlights

- New datasets expand evidence on concrete free thermal strain response in fire
- Bayesian updating quantifies uncertainties in concrete free thermal strain
- Coefficients show strong correlation, best modelled as multivariate Gaussian

1. Introduction

The traditional approach to structural fire design is prescriptive, in which standards or other guidance documents specify a required fire resistance rating and the criteria that a design must satisfy to achieve this (e.g., the required concrete cover or the minimum member size). These requirements reflect the experience and knowledge gained over time, often following disasters that indicated the need for updated prescriptive guidance. As a result, prescriptive design guidance focuses on common and existing types of structures, while novel designs are not covered [1]. For such structures, performance-based design, which explicitly quantifies the behaviour of the structure during the entire fire scenario, is more appropriate [2]. Furthermore, the prescriptive approach relies on the concept of standard fire. This is commonly a monotonically increasing fire,

such as ISO 834 [3], and does not include the decay and cooling phases, which are inherent parts of every natural fire. The need for the adoption of more realistic fire exposure has been indicated in the past two decades [4].

A performance-based structural fire design entails a detailed quantification of the behaviour of the structure during fire and relies on models for the thermal exposure, material properties, and structural interactions to do so. In this regard, the free thermal strain of concrete structures is of particular importance as restrained thermal expansion can result in fire-induced forces. This also applies during cooling, where the reversal of the thermal expansion alters the forces in the structure – possibly even in areas that remained unaffected by the fire. This can lead to a collapse in the cooling phase [5]. Hence, a model that is able to capture the free thermal expansion both during heating and cooling with sufficient accuracy is indispensable [6]. As the focus has historically been on the prescriptive approach to structural fire safety, many studies have focused on the free thermal strain during heating. This is also the case for concrete [7-13]. Studies focusing on the free thermal strain during cooling are largely absent in the literature, with [14] forming a notable exception. The state-of-the-art (SOTA) model for concrete thermal strain that considers both the heating and the cooling phase is the model implemented in the finite element software SAFIR [15], and is explained below in Section 2. Nevertheless, this model is based on a limited dataset for a single type of concrete [14], while also making reference to the work of Schneider [7] for additional data on the residual thermal strain of concrete. Hence, it would benefit from the inclusion of additional data to further validate and/or generalize the model.

When new data are collected, questions arise as to what approach should be followed in order to combine the new data with the prior model for the free thermal strain. In this regard, Bayesian inference provides a framework in which prior beliefs or information can be updated by introducing new information, while also allowing for a quantification of the uncertainty on the results [16,17]. For the thermal strain SOTA model [15], the prior information is captured in the model's coefficients, and in this paper the model is updated by incorporating information from newly performed experiments. In the following, first the model is explained, and the experiments are introduced. Subsequently, the Bayesian inference framework is described. Lastly, Bayesian inference is used to update the model, resulting in a probabilistic model for the free thermal strain of concrete that can be used for exposure to natural fires.

2. Thermal strain

2.1 Importance of thermal strain

The deformation of reinforced concrete elements is governed by the internal strains in the element. This 'total' strain, ε_{tot}, can be decomposed into the 'free thermal' strain, ε_{th}, the instantaneous 'stress-related' strain, ε_{σ}, and the 'transient' (creep) strain, ε_{tr}, according to Eq. (1), with T [°C] being the temperature, and σ [Pa] denoting stress:

$$\varepsilon_{tot} = \varepsilon_{th}(T) + \varepsilon_{\sigma}(\sigma, T) + \varepsilon_{tr}(\sigma, T) \quad (1)$$

When deformation is restrained, ε_{tot} is zero. This, however, does not imply that its constituent components are also zero. On the contrary, as ε_{th} is only a function of T, it is independent of the element's mechanical boundary conditions, and it needs to be compensated by ε_{σ} (and ε_{tr}). Hence, restrained thermal expansion can result in large internal stresses in the element and the magnitude of ε_{th}, combined with the amount of restraint, governs the magnitude of these stresses.

2.2 SAFIR thermal strain model

The SOTA free thermal strain model for concrete during heating and cooling [15] is based on the measured expansion of slowly heated concrete specimens with calcareous coarse aggregates and Rhine river sand [14]. It adopts the formulation of EN 1992-1-2:2004 [18] for the heating phase (Eq.(2)), while it interpolates between tabulated values for the residual thermal strain (Eq. (3)) [19]:

$$\varepsilon_{th,heat}(T) = \begin{cases} -1.8 \cdot 10^{-4} + 9 \cdot 10^{-6} T + 2.3 \cdot 10^{-1}\ T^3, & 20°C \leq T \leq 700\ °C \\ 14 \cdot 10^{-3}, & 700°C < T \leq 1200\ °C \end{cases} \quad (2)$$

$$\varepsilon_{th,cool}(t_r) = \varepsilon_{res}(T_{max}) + [\varepsilon_{EC2}(T_{max}) - \varepsilon_{res}(T_{max})][0.60 t_r + 0.40 t_r^2] \quad (3)$$

In these equations, $\varepsilon_{th,heat}$ and $\varepsilon_{th,cool}$ [-] are the free thermal strain during respectively heating and cooling, $\varepsilon_{res}(T_{max})$ [-] is the residual thermal strain at 20°C after heating to T_{max}, $\varepsilon_{EC2}(T_{max})$ [-] is the value of the free thermal strain during heating at T_{max}, and t_r is the normalized relative temperature, which is introduced in Eq. (4).

$$t_r = \frac{T-20}{T_{max}-20} \quad (4)$$

SAFIR obtains the value of $\varepsilon_{res}(T_{max})$ by linear interpolation from the values in Table 1.

Table 1. SAFIR residual thermal strain tabulated values [19].

Maximum temperature, T_{max} [°C]	20	300	400	600	800	≥ 900
Residual strain, ε_{res} ($\times 10^{-3}$) [-]	0.00	-0.58	-0.29	1.71	3.29	5.00

In view of updating the residual strain model, the tabulated data in Table 1 is approximated using the piecewise polynomial function of Eq. (5), which is a second degree polynomial for $T_{max} < 900$ °C and becomes constant for $T_{max} \geq 900\ °C$. The values for the parameters a and b are based on a least-squares fitting: $a = 1.28 \cdot 10^{-8}$ [°C^{-2}] and $b = -5.41 \cdot 10^{-6}$ [°C^{-1}].

$$\varepsilon_{res}(T_{max}) = \begin{cases} a \cdot (T_{max} - 20)^2 + b \cdot (T_{max} - 20), & T_{max} < 900\ °C \\ a \cdot (900 - 20)^2 + b \cdot (900 - 20), & T_{max} \geq 900\ °C \end{cases} \quad (5)$$

3. Experimental data

The dataset onto which Bayesian inference is performed, was gathered from 2 different experimental campaigns. The first experimental campaign focused on obtaining data for the residual thermal strain using a radiant panel setup. The second experimental campaign used a small furnace and measured the thermal displacement both during heating and cooling. Although the furnace tests also provide residual thermal strain values, the first setup has the advantage of being faster, allowing for an extensive dataset. For both setups, specimens with the same mixture were used. The mixture details can be found in Table 2.

Table 2. Concrete mixture details per m³. The aggregates have a siliceous nature.

Material	**Quantity**
Sand 0/4	927 kg
Granulates 2/8	497 kg
Granulates 8/16	577 kg

CEM I 52.5 N	300 kg
Water	150 kg
Superplasticizer Master Glenium 20%	0.84 L

3.1 HIFREP tests

The first test setup involved concrete cubes with a side length of 10 cm, insulated on the sides and the bottom and heated by the HIFREP [20] (an infrared electric radiant panel) from the top, introducing a nearly 1-dimensional temperature gradient in the specimens. At the time of testing, the cubes were approximately 3 months old. They were cured for 4 weeks in an environment of 20°C and a relative humidity (RH) of 99%. Subsequently, they were left at ambient conditions. The insulation consisted of 2.5 cm of ceramic wool and 2.5 cm of calcium silicate board ('rigid encasement'). Their thermal properties are provided in Table 3. Four cubes were tested simultaneously in a 2 by 2 arrangement and the incident radiative heat flux was measured with a water-cooled Schmidt-Boelter type heat flux gauge [21] in the middle between the four cubes. Ten experimental runs with four cubes each were conducted (total number of samples is 40). No repetitions were performed. A schematic overview of the test setup is provided in Fig. 1 (left). Thermocouples were originally placed inside the specimens during casting. However, due to poor control over their exact positioning, these data were not deemed reliable and were therefore discarded. Instead, thermocouples were installed on the side of the specimens using aluminium tape, enabling much more precise control of their locations.

Table 3. Thermal properties of the insulations materials used in the HIFREP tests [22], [23].

	Ceramic wool	**Calcium silicate board**
Thermal conductivity [W/mK]	0.05 (200 °C); 0.08 (400 °C); 0.12 (600 °C); 0.18 (800 °C); 0.25 (1000 °C)	0.12 (400 °C); 0.15 (600 °C); 0.17 (800 °C)
Specific heat [J/kgK]	-	800-1200
Density [kg/m³]	128	255

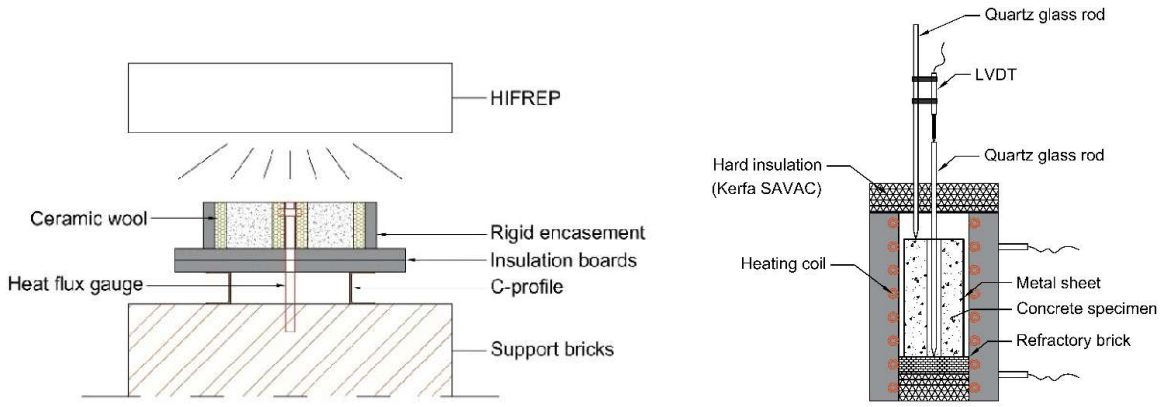


Fig. 1.Schematic overview of HIFREP tests (left) and furnace test setup (right).

After heating (each experiment considered a constant heat flux between 80 and 133 kW/m² and duration between 1.5 and 2.5 h), the specimens were left to cool down to ambient temperature by natural cooling, after which the residual expansion of the specimens was measured by means of a calliper (accuracy of ± 0.01 mm; the mean value of 8 measurements was used). This value was

then corrected for the residual bending, expressed by the curvature (φ), introduced by the thermal gradients inside the specimens. The correction for φ, essentially comes down to subtracting the distance Δy from the measured value y, resulting in the real height x of the specimen, as demonstrated in Fig. 2. The parameter φ is evaluated by considering (i) the Bernoulli assumption that plane sections remain plane after deformation, (ii) the thermal strain model from Section 2, (iii) the condition of no net residual axial forces and bending moments in the section and (iv) a maximum temperature profile as obtained from SAFIR [15, 24]. Using basic trigonometric operations, Eq. (6) links Δy to φ, and substituting the evaluated φ yields Δy values that ranged from 0.04 to 0.06 mm in the current tests. The test results are visualized in Fig. 3 (left), in which the error bars represent the aggregated results of the four cubes tested in that run.

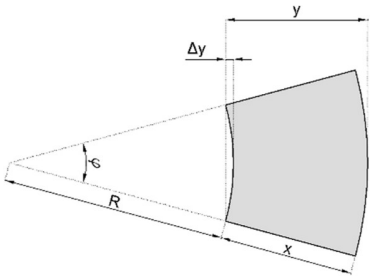


Fig. 2. Calliper measurement correction for specimen curvature

$$\Delta y = R \cdot \left(1 - \cos\frac{\varphi}{2}\right) \tag{6}$$

The SAFIR (version 2022.d.7) modelling was done to obtain the maximum temperature over the height of the specimen, and input parameters (see below) were adjusted in such a way that the difference between the prediction by SAFIR and the experimentally measured temperatures was minimized. The residual thermal strain model was applied to the maximum temperature profile to obtain the residual displacement. Thermal boundary conditions were based on measured heat flux with reradiation to 200 °C during heating and 20 °C during cooling. Concrete was modelled with SILCONC_EN (density 2300 kg/m³, thermal conductivity parameter = 1). The board and wool had specific heat capacities of 1000 and 500 J/kgK, and dry densities of 255 and 100 kg/m³, respectively. Thermal conductivity was not fixed but optimized by least squares to approximate the specimen's measured maximum temperature profile as closely as possible (0.02–0.1 W/mK for the board; 0.02–0.2 W/mK for the wool). Other parameters were left to the default values.

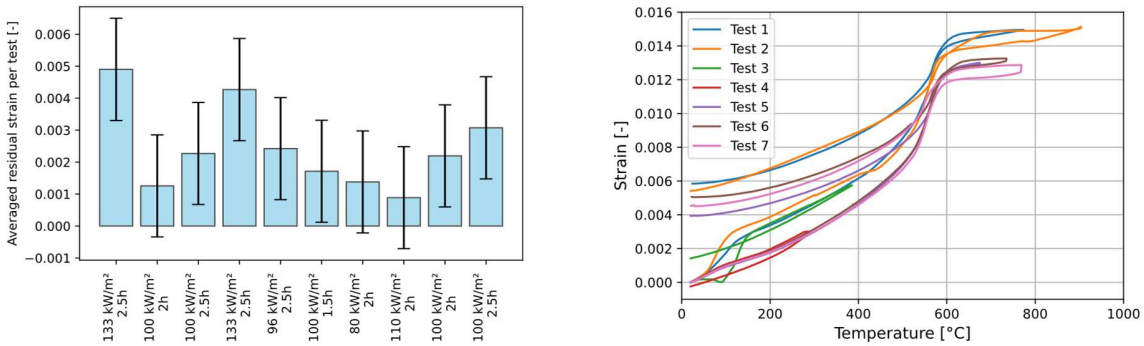


Fig. 3. Summary of the experimental results of the HIFREP tests (left) and the furnace tests (right).

3.2 Furnace tests

The second test setup consisted of a 200 mm tall cylindrical concrete specimen with a 100 mm diameter and a 24 mm diameter core drilled in its centre, placed inside a cylindrical furnace (8 coils at 5 cm interval embedded in 5 cm of Kerfa SAVAC insulation material) with an internal diameter just exceeding 100 mm. At the time of testing, the specimens were approximately six months old, of which 4 weeks were spend at 20°C and 99% RH, after which they were cured further in ordinary laboratory conditions. Each specimen was covered with a 0.4 mm thick metal sheet to obtain a more uniform temperature over the specimen. The furnace temperature was gradually increased at a rate of 0.5 °C per minute to obtain a nearly uniform temperature inside the specimen. The temperature was controlled with a K-type thermocouple positioned between the outer edge of the specimen and the metal sheet, while a second thermocouple attached to the inner surface (in the core) measured the concrete temperature. The thermally-induced displacement of the top surface of the specimen was monitored by means of a Linear Variable Differential Transformer (LVDT), which measured the relative displacement between a quartz glass rod positioned on the top surface of the specimen and a rod positioned on the base of the furnace through the drilled core. The reading of the inner thermocouple was used as a reference for the concrete temperature as the LVDT position was very close to the position of this thermocouple. A schematic visualization of the test setup is provided in Fig. 1 (right), while the experimental results are given in Fig. 3 (right). For each strain model updated (residual, cooling, or heating), the data from these tests are either the residual deformation or the corresponding part of the full deformation–time curve.

4. Bayesian inference

4.1 Basics of Bayesian inference

Bayesian inference is an approach that updates the prior belief or probability of a hypothesis by incorporating new information or data [17]. The entire method is built around Bayes' theorem, which states:

$$P(H|E) = \frac{P(E|H) \cdot P(H)}{P(E)} \tag{7}$$

Where H is the prior belief or hypothesis, E denotes the new information or evidence, and P stands for the probability. Bayes' theorem states that the posterior probability given the evidence $P(H|E)$ can be calculated from the likelihood $P(E|H)$ (i.e., the probability of observing E given H), the prior probability of the hypothesis $P(H)$, and the marginal likelihood $P(E)$ (i.e., the probability of observing E irrespective of H).

A direct implementation of Eq. (7) is impractical as the marginal likelihood $P(E)$ is hard to evaluate for most practical applications. Instead, special algorithms can be employed to avoid the direct calculation of $P(E)$. For the current study, the Metropolis-Hastings algorithm – a Markov chain Monte Carlo method – is used [25, 26].

Bayesian inference enables the updating of parameter probability distributions, including hyperparameters, to account for uncertainties, even when they are not precisely known [17]. The prior probability density functions incorporate prior knowledge and engineering judgment. While priors influence the posterior distributions, their effect diminishes as more informative data becomes available. The following sections explore case-specific considerations for applying Bayesian inference to thermal strains. A detailed step-by-step guide for Bayesian updating in a fire safety context, including calculation methods, is available in [27].

4.2 Prior distributions

The Bayesian inference methodology starts with defining the prior distributions for the parameters of interest. Here, the parameters of interest are the coefficients of the thermal strain model of SAFIR, as introduced in Section 2.2. There are several approaches to defining the prior distributions, such as literature data, visual inspection (e.g., plotting of multiple realizations), or engineering judgement. Here, the choice for the prior distributions is based on a combination of visual inspection and engineering judgement, as the background data of the EN 1992-1-2 thermal strain model is not readily available, and the dataset during and after cooling is limited. Rewriting Eq. (2), Eq.(3) and Eq. (5) in parametrized form results in Eq. (8), Eq. (9) and Eq. (10) respectively. In these equations, a to e are the coefficients of the thermal strain model [1/°C^n], ΔT_{plat} and $\Delta T_{plat,res}$ are the plateau temperature increases in respectively the heating and residual thermal strain models [°C], ΔT and ΔT_{max} are respectively the temperature increase and maximum temperature increase from ambient [°C]. In the limit $c = 2.3 \cdot 10^{-1}\ \frac{1}{°C^3}$, $d = 1.38 \cdot 10^{-9} \frac{1}{°C^2}$, and $e = 9.03 \cdot 10^{-6} \frac{1}{°C}$, Eq. (8) reduces to Eq. (2):

$$\varepsilon_{th,heat}(\Delta T) = \begin{cases} c \cdot \Delta T^3 + d \cdot \Delta T^2 + e \cdot \Delta T, & 0°C \leq \Delta T \leq \Delta T_{plat} \\ c \cdot \Delta T_{plat}^3 + d \cdot \Delta T_{plat}^2 + e \cdot \Delta T_{plat}, & \Delta T_{plat} < \Delta T \leq 1180\ °C \end{cases} \quad (8)$$

$$\varepsilon_{th,cool}(t_r) = \varepsilon_{res}(\Delta T_{max}) + \left[\varepsilon_{th,heat}(\Delta T_{max}) - \varepsilon_{res}(\Delta T_{max})\right][r t_r + (1-r) t_r^2] \quad (9)$$

$$\varepsilon_{res}(\Delta T_{max}) = \begin{cases} a \cdot \Delta T_{max}^2 + b \cdot \Delta T_{max}, & \Delta T_{max} < \Delta T_{plat,res} \\ a \cdot \Delta T_{plat,res}^2 + b \cdot \Delta T_{plat,res}, & \Delta T_{max} \geq \Delta T_{plat,res} \end{cases} \quad (10)$$

The prior distributions of Table 4 are assigned to the model's coefficients. For the coefficients a and c, a lognormal distribution was chosen to maintain the convexity of the thermal strains models they are part of. As an example, Fig. 4 (left) visualizes the expected values and quantiles of the prior predictive models for concrete subject to a heating and cooling cycle reaching 800 °C.

Table 4. Prior probability density functions for the parameters of the thermal strain model.

Parameter	Unit	Distribution type	Mean	Standard deviation	Lower bound	Upper bound
c	°C^{-3}	Lognormal	$3 \cdot 10^{-11}$	$1.5 \cdot 10^{-11}$	-	-
d	°C^{-2}	Normal	$1.38 \cdot 10^{-9}$	$0.69 \cdot 10^{-9}$	-	-
e	°C^{-1}	Normal	$9 \cdot 10^{-6}$	$4.5 \cdot 10^{-6}$	-	-
ΔT_{plat}	°C	Uniform	-	-	380	780
a	°C^{-2}	Lognormal	$1.28 \cdot 10^{-8}$	$0.38 \cdot 10^{-8}$	-	-
b	°C^{-1}	Normal	$-5.41 \cdot 10^{-6}$	$1.62 \cdot 10^{-6}$	-	-
$\Delta T_{plat,res}$	°C	Uniform	-	-	500	1200
r	-	Uniform	-	-	0	1

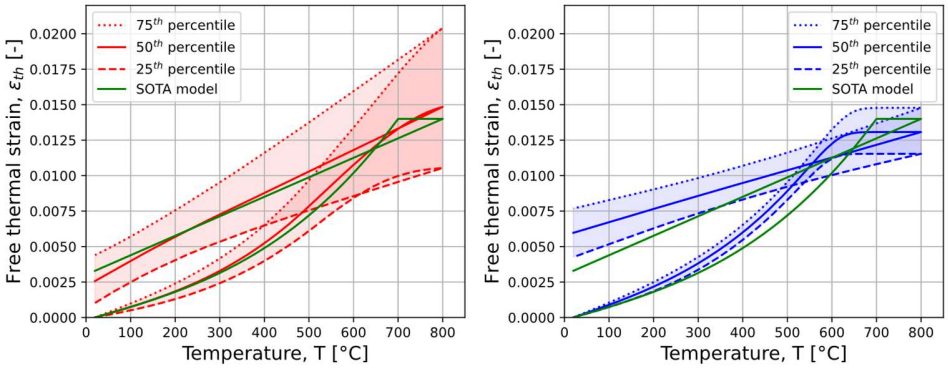


Fig. 4. Model prediction and associated uncertainty band compared to the SAFIR model based on prior (left) and posterior distributions (right), based on 10^5 Monte Carlo simulations for $T_{max} = 800$ °C.

4.3 Forwarding models

In Bayesian inference, the forwarding model is the model that links the parameters that are to be updated to the data that is introduced as new information [27]. The forwarding models in the current study implement Eqs. (8)-(10) for the calculation of the residual deformation and time-dependent deformation of the samples. As data was obtained from two test campaigns with a different test setup (details provided in Section 3), the following implementations are used:

- HIFREP setup: Cubes were discretized into 25 slices (4 mm each). SAFIR provided the maximum temperature profile over the height. Residual thermal strain was applied to each slice, multiplied by slice thickness, and summed to obtain the cube's total residual displacement.
- Furnace setup: The concrete cylinder was slowly heated, allowing a quasi-uniform temperature assumption throughout the test. The residual thermal strain model was applied to the whole specimen, and strain was converted to time-dependent displacement by multiplying with the cylinder's original height.

4.4 Likelihood

The update of the thermal strain model parameters is performed using Bayes' theorem (Eq. (7)), which connects the posterior probability f'' ([-] or [1/m]) of the parameters given the observed data (measured strain or displacement), with the likelihood of the data given the parameters, L [-], and the prior probability of the parameters, f' ([-] or [1/m]) [27]:

$$f''(\boldsymbol{p}|\boldsymbol{d}) \sim L(\boldsymbol{d}|\boldsymbol{p}) \cdot f'(\boldsymbol{p}) \tag{11}$$

$\boldsymbol{p}$ and $\boldsymbol{d}$ are vectors of the parameters and the data respectively.

The likelihood, L, is generally calculated as follows:

$$L = \prod_{i=1}^{n} (2\pi\sigma_i)^{-\frac{1}{2}} \exp\left(-\frac{(d_i - M_{d,i})^2}{2\sigma_i^2}\right) \tag{12}$$

In Eq. (12), σ_i is the standard deviation of the normally distributed error for the measured quantity with mean 0, d_i is the measured value, $M_{d,i}$ is the model result, and n is the number of datapoints. The likelihood should consider the available information, with the normal distribution being the maximum entropy distribution for a given mean and standard deviation. Therefore, the normal

distribution is the obvious choice to express the likelihood in the absence of a specific reason to adopt a different one [28, 29].

The estimation of σ_i is complex, as it reflects multiple sources of uncertainty. For the HIFREP tests, these include calliper measurements, bending correction (Bernoulli assumption), SAFIR temperature predictions, and measured heat fluxes. For the furnace tests, they include temperature measurement, temperature homogeneity in the specimen, and LVDT accuracy. In addition, it should be noted that an LVDT provides a point measurement and cannot be used directly for the entire surface. One option for the specification of σ_i is to update σ_i within the inference process though this increases computational cost and risks overfitting by compensating model inadequacies [17]. Given the regression-based nature of the models, a conservative σ_i was adopted (see Results section), except when updating actual parameters (e.g., ΔT_{plat}), where σ_i was treated as variable.

5. Results

5.1 Residual thermal strain model

The Bayesian inference for the residual thermal strain is split into two parts as there are two datasets with different forwarding models. In the following, the HIFREP data is considered first. It is important to note that the final posterior distributions are independent of the order of the inference (i.e., the same results would be obtained in case the furnace data was considered first, followed by the HIFREP data).

5.1.1 Inference on HIFREP test data

The results of the Bayesian inference on the residual thermal strain parameters considering the HIFREP test data and using 0.3 mm as standard deviation for the likelihood function are provided in Fig. 5. From these visualizations, it is clear that the data was informative for the parameters a (Fig. 5 (left)) and b (Fig. 5 (middle)), but not for $\Delta T_{plat,res}$ (Fig. 5 (right)). While the posterior distributions for a and b are clearly narrower than the priors and can be approximated with a normal distribution ('Posterior approx.' in the figure), the posterior distribution of $\Delta T_{plat,res}$ is only slightly more informative than the uniform prior. The likelihood of $\Delta T_{plat,res}$ being below 750 °C has reduced, but there is no difference in posterior probability for plateau temperatures higher than approximately 850 °C. This is logical as the test data does not provide information for such high temperatures. The outcomes are summarized in Table 5.

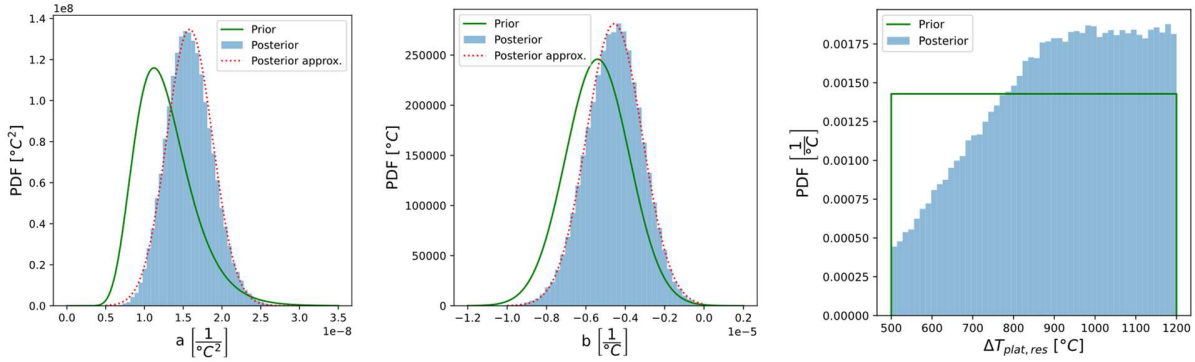


Fig. 5. Results for the residual thermal strain parameters a (left), b (middle) and $\Delta T_{plat,res}$ (right) considering HIFREP data.

Table 5. Marginal posterior distributions after Bayesian inference on HIFREP data.

Parameter	Unit	Distribution type	Mean	Standard deviation
a	$°C^{-2}$	Normal	$1.58 \cdot 10^{-8}$	$2.96 \cdot 10^{-9}$
b	$°C^{-1}$	Normal	$-4.56 \cdot 10^{-6}$	$1.42 \cdot 10^{-6}$
$\Delta T_{plat,res}$	°C	-	911.04	181.07

The posterior (marginal) distributions of a and b should, however, not be considered as independent distributions. The 2D histograms of the results in Fig. 6 indicate that there is a linear correlation between the two parameters, while there is no correlation with $\Delta T_{plat,res}$. Hence, instead of sampling from the marginal distributions independently, sampling should be done from a joint posterior distribution. For this specific case, a multivariate normal distribution (Pearson's correlation coefficient of -0.79) would be appropriate as the marginal distributions are both normal distributions.

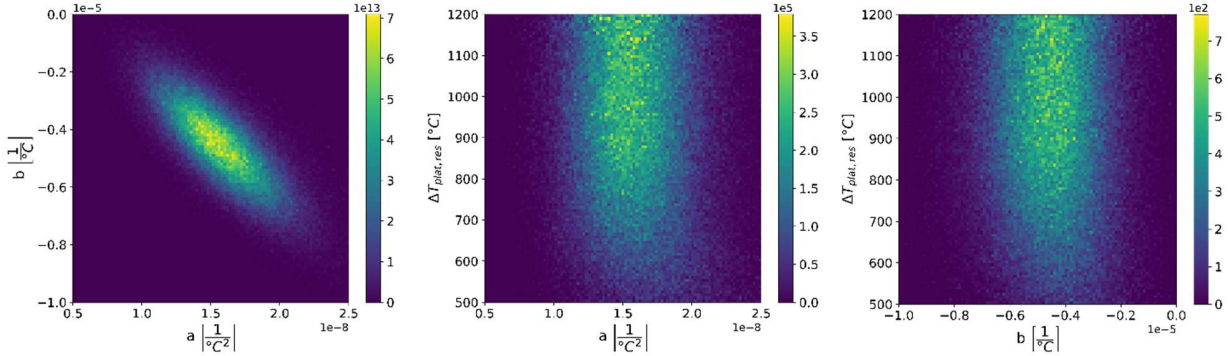


Fig. 6. Correlation between a and b (left), a and $\Delta T_{plat,res}$ (middle), and b and $\Delta T_{plat,res}$ (right) in the residual thermal strain model considering HIFREP data.

5.1.2 Inference on furnace test data

In order to incorporate all the information from both the HIFREP and the furnace tests in the Bayesian inference, the priors for the inference on the furnace tests data are the posteriors of the inference of the HIFREP data for the parameters a and b, including their correlation (they are modelled as a multivariate Gaussian distribution). As a starting point for $\Delta T_{plat,res}$, the same uniform distribution as for the inference on the HIFREP test data was used, as it did not provide significant information. The analysis was carried out using a strain value of 0.002 for the standard deviation in the likelihood function. The results of the inference process are provided in Fig. 7, from which it is clear that the inclusion of the additional data has no significant effect on the marginal distributions of a (Fig. 7 (left)) and b (Fig. 7 (middle)). For a, a slight shift of the distribution to the left (i.e., lower values) can be noticed, while the distribution of b has hardly changed. The update of $\Delta T_{plat,res}$ (Fig. 7 (right)) provides a clearer picture in this case. A peak can be observed around a temperature increase of 750 °C and the distribution seems to be approximately Gaussian, but the update above 880 °C is limited and independent of temperature as this was the maximum temperature increase observed in the experiments. The results are summarized in Table 6.

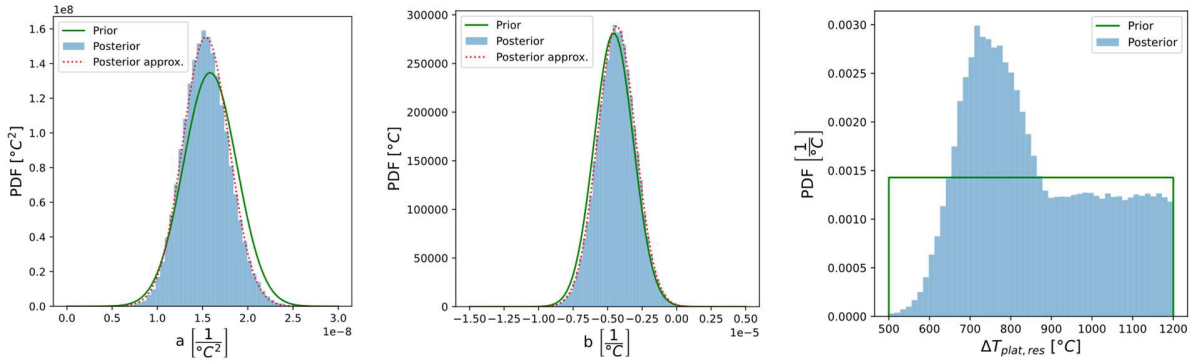


Fig. 7. Results for residual thermal strain parameters a (left), b (middle) and $\Delta T_{plat,res}$ (right) considering HIFREP and furnace test data.

Table 6. Marginal posterior distributions after Bayesian inference on HIFREP and furnace data.

Parameter	Unit	Distribution type	Mean	Standard deviation	Covariance matrix
a	$°C^{-2}$	Normal	$1.54 \cdot 10^{-8}$	$2.57 \cdot 10^{-9}$	$\begin{bmatrix} 6.60 \cdot 10^{-18} & 2.99 \cdot 10^{-15} \\ 2.99 \cdot 10^{-15} & 1.91 \cdot 10^{-12} \end{bmatrix}$
b	$°C^{-1}$	Normal	$-4.35 \cdot 10^{-6}$	$1.38 \cdot 10^{-6}$	
$\Delta T_{plat,res}$	°C	-	861.35	165.67	

The results of the inference on the furnace test data indicate a clear correlation between the parameters a and b, as demonstrated in **Error! Reference source not found.**. Even though their marginal distributions did not change much by the second iteration of inference, their correlation is stronger (correlation coefficient of -0.84 as compared to -0.79 after inference on only the HIFREP data), resulting in an improved model overall. In this regard, **Error! Reference source not found.** visualizes the performance of the updated model compared to the model with the prior probability density functions. For comparison, the residual strain values from the furnace test have been added to the figure. As no practically applicable distribution for $\Delta T_{plat,res}$ could be obtained, the current SOTA model value of 880°C is maintained.

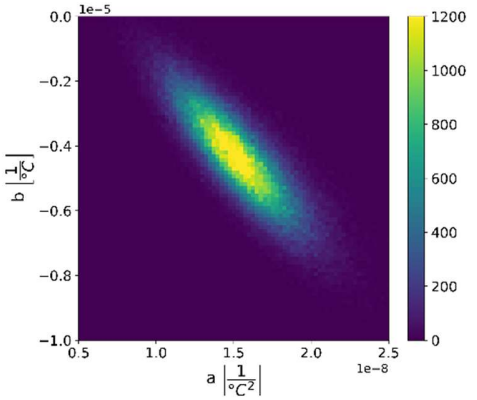


Fig. 8. Correlation between residual thermal strain parameters a and b after inference on HIFREP and furnace data.

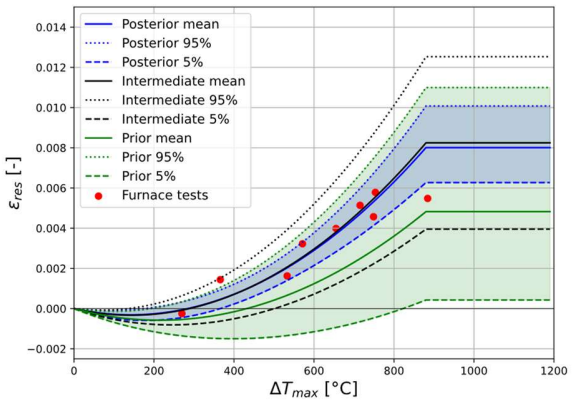


Fig. 9. Prior, intermediate (i.e., posterior with only HIFREP data) and posterior model for the residual thermal strain of siliceous concrete. The update of $\Delta T_{plat,res}$ is not considered.

5.2 Thermal strain model during cooling

The data used to update parameter r (see Eq. (9)) are not single, independent datapoints. Rather, the data are a set of temperature-thermal strain datapoints, constructed from two time series: a time series of recorded temperatures and a time series of measured displacements. The combination of these datasets results in the desired temperature-displacement data. Performing Bayesian updating with series of datapoints is more difficult than using single datapoints because the datapoints of a set are correlated and thus not fully independent of each other. To resolve this issue, the value of r is derived from curve fitting to the experimental data (using a nonlinear least-squares approach). This value is subsequently used to perform Bayesian updating with. The uncertainty on the value of r resulting from this approach is considered in the Bayesian updating process.

The comparison between the experimental temperature-displacement data and the curves obtained from curve fitting indicated that a second degree polynomial is not adequate for temperature-strain curves that reach to the plateau temperature increase, $\Delta T_{plat,res}$, as indicated in Fig. 10. Changing the second degree term to a fourth degree was found to be a better alternative for these cases, while also being suitable for cases in which $\Delta T_{plat,res}$ is not reached. The cooling phase formulation of the thermal strain of Eq. (9) is updated to Eq. (12). Note that this change does not affect the choice of the prior distribution of r as it still needs to be between 0 and 1 to satisfy the boundary conditions.

$$\varepsilon_{th}(T) = \varepsilon_{res}(T_{max}) + [\varepsilon_{EC}\ (T_{max}) - \varepsilon_{res}(T_{max})][rt_r + (1-r)t_r^4] \quad (12)$$

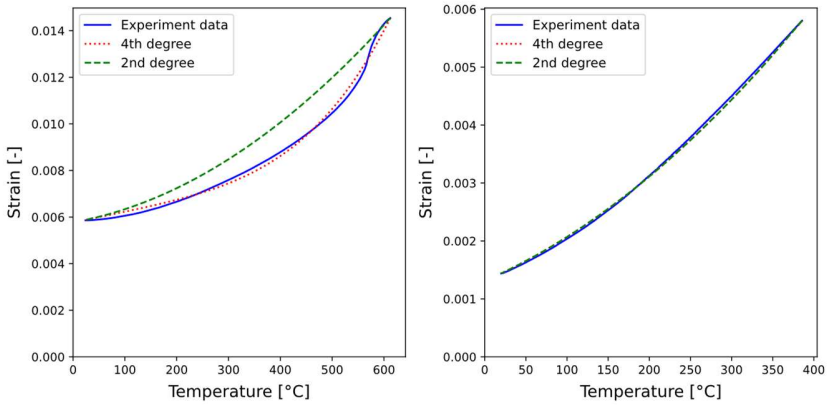


Fig. 10. Comparison between a second a fourth degree term in the formulation of the thermal strain during cooling for a case in which $\Delta T_{plat,res}$ is reached (left) and a case in which $\Delta T_{plat,res}$ is not reached (right).

The result of the Bayesian updating process on the shape parameter, r, is provided in Fig. 11 and considers a standard deviation for the likelihood function of 0.05. This standard deviation is based on the variance obtained in the curve fitting process. The prior uniform distribution has transformed into a narrow posterior distribution that can be very well approximated with a normal distribution centred around 0.45 with a standard deviation of 0.02.

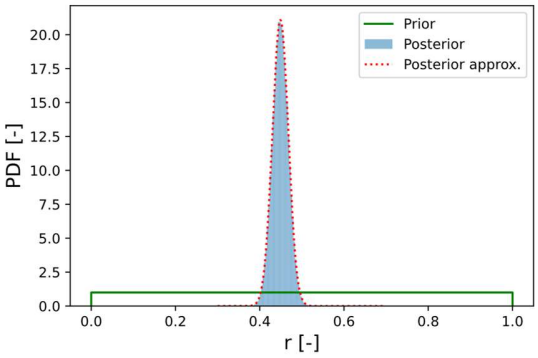


Fig. 11. Prior and posterior distribution for the shape parameter, r.

5.3 Thermal strain model during heating

The data used for the inference of the strain model during heating is based on temperature-displacement series rather than single datapoints. This is thus similar to the Bayesian inference described above for the thermal strain model during cooling (the shape parameter, r). While the approach using least-squares estimations of r was a feasible approach, it is hard to apply when multiple interdependent parameters (c, d and e) need to be estimated. As an alternative, an autoregressive (AR) model is applied to the temperature-displacement datasets. AR models take into account the correlation between steps (usually time steps, but here temperature steps) [30]. In this study, an AR model of degree 1 (hereafter denoted as AR(1)) is used, meaning that only the previous time step is considered, according to $x_i = \rho x_{i-1} + \epsilon_i$, with ρ [-] the AR(1) coefficient indicating the relationship between steps and ϵ_i [-] the random error at step i, usually following a normal distribution with mean 0 and standard deviation σ.

Autoregressive (AR) models assume that the data is stationary — meaning that the statistical properties, such as mean and variance, remain constant over time. However, because the data exhibits an increasing trend, this assumption is violated. To address this, the AR(1) model is applied not to the raw data, but to the residuals (the differences between the measured values and the predictions from the model) [31]. This isolates the stationary component if the error is absolute and not relative. Since the measurements were obtained using an LVDT, and the uncertainty is specified as a percentage of the full measurement range, the resulting uncertainty should be regarded as an absolute error. Hence, this allows the AR(1) model to be used appropriately. The result of the Bayesian inference process using this approach is provided in Fig. 12 and also includes the AR(1) hyperparameter ρ (Fig. 12d), of which the prior was a uniform distribution with lower limit 0 and upper limit 3. The standard deviation of the error ϵ_i is not considered in the inference process and is kept constant at 0.003. To allow for values of ρ bigger than 1, the first datapoint is not considered stationary, i.e., the modelling does not assume a process that has been running forever in a stationary regime. Instead it just starts from the first datapoint.

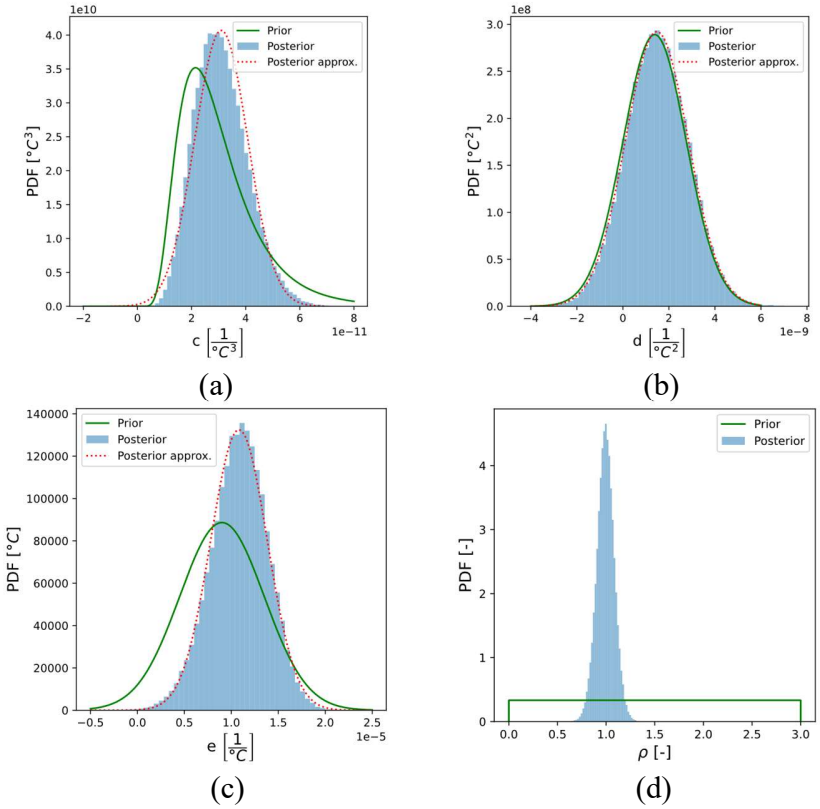


Fig. 12. Prior and posterior marginal distributions for the coefficients (a) c, (b) d, and (c) e of the thermal strain model during heating, and (d) the correlation parameter, ρ, of the AR(1) model.

Based on the posterior of ρ, the probability of $\rho < 1$ (i.e., the AR(1) process is stationary) is 0.53. This implies that the probability of the AR(1) process being non-stationary is 0.47. Hence, it is statistically uncertain whether the residuals are stationary or not. This usually indicates that the model is lacking a slowly evolving component [31], [32], which may be considered as a bias, possibly temperature-dependent in this case. This is also the reason why the standard deviation of the error ϵ_i is not explicitly modelled: it would tend to zero (overfitting to overcome the bias in the regression model) and the updating process would be stopped. Nevertheless, proposing a novel model is outside the scope of the current work, which aims at updating the coefficients of the existing model.

The marginal posterior distributions of the model parameters, c, d and e, can be well approximated with normal distributions. The details of these distributions can be found in Table 7. For the coefficient d, it can be noted that the difference between the prior and posterior distributions is very small. This is because its contribution is limited compared to the other terms (especially the third degree one). Calculating the Z-statistic (ratio of mean and standard deviation), results in a value of 1.1. From this, the 2-sided p-value can be calculated, amounting to 0.27, which is much larger than the conventional threshold of 0.05. Hence, the hypothesis that d is essentially zero and that the second-degree term could be omitted from the equation, is accepted. Additionally, due to their correlation, the posteriors of c and e should not be considered independently, but as a joint posterior distribution.

Table 7. Marginal posterior distributions for thermal strain during heating model coefficients.

Parameter	Unit	Distribution type	Mean	Standard deviation	Covariance matrix
c	$°C^{-3}$	Normal	$3.06 \cdot 10^{-11}$	$9.63 \cdot 10^{-12}$	$\begin{bmatrix} 9.27 \cdot 10^{-23} & -2.12 \cdot 10^{-17} \\ -2.12 \cdot 10^{-17} & 8.21 \cdot 10^{-12} \end{bmatrix}$
e	$°C^{-1}$	Normal	$1.08 \cdot 10^{-5}$	$2.86 \cdot 10^{-6}$	
d	$°C^{-2}$	Normal	$1.48 \cdot 10^{-9}$	$1.35 \cdot 10^{-9}$	

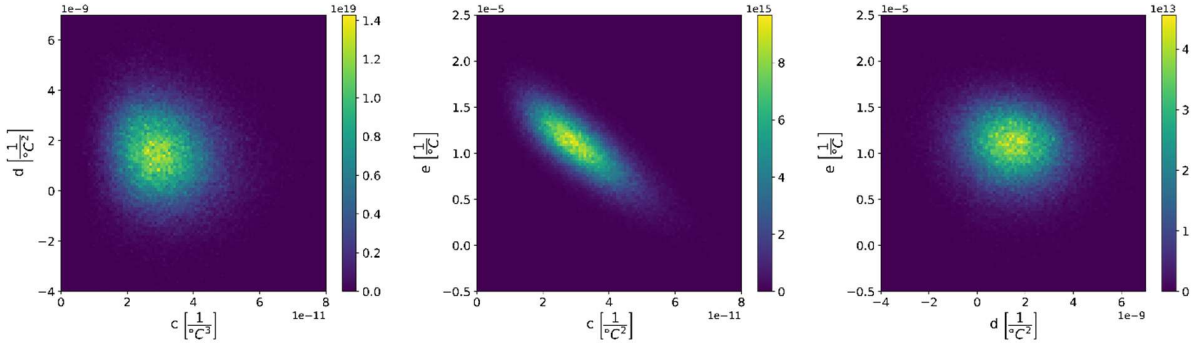


Fig. 13. Correlation between the coefficients c and d (left), c and e (middle), and d and e (right) of the thermal strain model during heating.

The last parameter of the heating model for the thermal strains that needs to be considered is the temperature increase at which the plateau starts, ΔT_{plat}. As can be observed in Fig. 14, the 'plateau' behaviour of the model does not align with the observations in the furnace tests as the rate of change gradually reduces but never becomes really zero during heating. In order to define a value of ΔT_{plat} for each experimental observation, a moving average is taken of the thermal strain and a threshold for the rate of change is adopted as criterion for having reached the plateau. This approach is however very sensitive to the considered window size for the moving average and the set threshold. As a consequence, the plateau temperature is ill-defined. To take this into account, the standard deviation, σ, for the likelihood is explicitly considered as variable in the Bayesian inference process. This standard deviation, σ, cannot be readily assessed and therefore a very uninformative prior distribution is adopted: a uniform distribution between 0 and 500 °C. The results of the Bayesian inference process are provided in Fig. 15 and indicate that the plateau temperature increase can be described probabilistically by a normal distribution with a mean value of 589.2 °C and a standard deviation of 45.2 °C. The mean value of the standard deviation of the likelihood after the inference process is found to be 209.07 °C, indicating the large spread that can be expected from the approach to determine ΔT_{plat}.

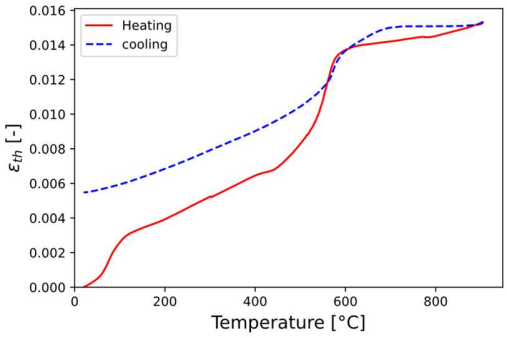


Fig. 14. Example of measured thermal strain in furnace test.

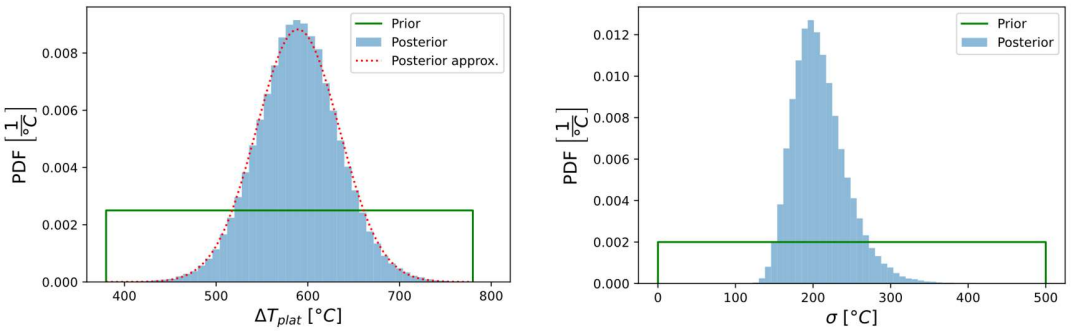


Fig. 15. Prior and posterior distributions from the Bayesian inference on ΔT_{plat} for ΔT_{plat} itself (left) and the standard deviation of the likelihood, σ (right).

Fig. 4 (right) provides an illustration of the behaviour encoded by the updated model compared to the behaviour for the model based on the prior probability density functions, for concrete heated to 800 °C. It can be observed that the 25th and 75th percentiles of the posterior model are much closer together than those of the prior model, indicating a stronger belief in the actual value of the thermal strain for the specific type of concrete in this study.

6. Discussion

In both the heating and residual thermal strain models, the posterior model coefficients have been found to be correlated. As a result, sampling cannot be done from the marginal posterior distributions independently, but from a joint posterior distribution that takes their correlation into account. The correlation between the parameters could have been anticipated as each datapoint results in a linear relationship between the two parameters (a and b, or c and e), see Eqs. (10) and (8). Their correlation is thus inherent to the model definition.

The inference on the value of the plateau temperature increase in the residual thermal strain model, $\Delta T_{plat,res}$, did not fully achieve its objective as the prior distribution was only updated to a limited extent by the incorporation of the data. As $\Delta T_{plat,res}$ cannot be measured directly, it has to be deduced indirectly from the data. In this regard, the data from the HIFREP tests were not very informative due to the lower temperature in most of the specimen (only part of the specimen reached $\Delta T_{plat,res}$, with a limited overall contribution to the residual deformation). Also the data from the furnace tests were limited to a maximum temperature slightly above 900 °C (due to equipment constraints), which was too low to obtain a complete update. It is, therefore, recommended that additional tests be performed with maximum temperatures that exceed the current maximum (904 °C). On the other hand, the limited reduction in uncertainty obtained through the Bayesian updating should also be recognized as a strength of the methodology. Thanks to the mathematically rigorous approach, biased subjective interpretation is avoided.

A sensitivity analysis of the assumptions in Table 4 has been performed by adopting less-informative priors for all parameters (i.e., higher standard deviations). The results indicate that similar posterior distributions are obtained, but that more samples and computational power are needed to achieve these results. The posterior distributions are also less narrow than the ones presented above in the paper, as less prior information was provided.

The current study aimed at improving existing deterministic models for the free thermal strain of siliceous concrete, both during heating and cooling, in a mathematically rigorous and transparent way. The focus was on confirming/improving the coefficient values within the models, not on

improving the model architecture itself. Nevertheless, the outcomes of the Bayesian inference process have indicated that the model for the free thermal strain during heating, as given in EN 1992-1-2:2004, is not capable of fully explaining the observed behaviour. This is, however, not surprising as the models are merely regression functions applied to existing datasets, essentially without considering the physics behind the real phenomena that govern the thermal expansion, such as the competition between the aggregates that want to expand and the cement paste that wants to shrink, moisture evaporation, and dehydration of the cement paste [33]. This is inherent to many of the regression-based models in engineering and a point of attention when performing Bayesian inference on such models.

Probabilistic models describe the likelihood of different outcomes instead of yielding a single fixed value, the latter being the case with deterministic models. This allows for uncertainties to be explicitly quantified and forms the basis for reliability-based design, which underpins modern building codes. By defining the appropriate probability distribution together with its relevant parameters, such models can be directly implemented in code provisions. A complete probabilistic assessment may be carried out using Monte Carlo simulation, while semi-probabilistic methods, e.g., using prescribed design values, offer a practical alternative when uncertainties are well characterized but still non-negligible. Purely deterministic approaches are only suitable when uncertainties are minimal, a condition that is rarely met in structural fire engineering.

7. Conclusions

In this study, the deterministic state-of-the-art model for the free thermal strain of concrete during and after fire exposure was enhanced by incorporating new experimental data using Bayesian inference.

For the free thermal strain during heating in a fire, an autoregressive model of order 1 was employed to account for the correlation between datapoints within individual experiments. The results demonstrate a minor systematic bias in the model, which is consistent with expectations, as regression-based approaches inherently lack representation of the underlying physical mechanisms. Nonetheless, a reliable update of the model coefficients (c and e) was achieved, revealing a strong correlation between them and reinforcing the need to model them jointly using a multivariate distribution. The updated estimate of the plateau temperature increase, ΔT_{plat}, also provided valuable insight into the probabilistic nature of this parameter.

The post-fire residual thermal strain is represented by a two-parameter quadratic function of ΔT_{max} up to a plateau, beyond which it remains constant. The inference results for the model parameters show that the coefficients (a and b) are correlated and can be effectively represented by a multivariate Gaussian distribution. However, the update of the plateau temperature increase, $\Delta T_{plat,res}$, was limited. The HIFREP fire test data were not informative enough to yield meaningful estimates for this parameter, and the furnace test data did not reach sufficiently high temperatures to support a more informative update. Therefore, the current suggestion to have the plateau starting at a temperature increase of 880 °C is maintained. Future research should focus on improving this suggestion by including data from furnace tests at higher temperatures (over 1000 °C).

For the free thermal strain during cooling, the parameter r, which governs the transition between the hot free thermal strain and the residual free thermal strain, was inferred using non-linear least-squares estimations. This procedure was effective, yielding a narrow posterior distribution that is approximately normal.

Acknowledgements

This research has been funded by Research Foundation of Flanders (FWO) within the scope of the research project (Grant number 1137123N) "Characterization of the thermal exposure and material properties of concrete during the fire decay phase for performance-based structural fire engineering". In addition, Florian Put would like to acknowledge the travel grant (Grant number V462724N) received by FWO to perform the furnace tests at Politecnico di Milano. Dr Lucherini would also like to gratefully acknowledge the financial support for the FRISSBE project within the European Union's Horizon 2020 research and innovation program (GA 952395). The authors would like to thank ir. Thibeau Margo for his assistance in the execution of the HIFREP test campaign.

References

[1] G. Spinardi, L. Bisby, and J. Torero, 'A Review of Sociological Issues in Fire Safety Regulation', *Fire Technol.*, vol. 53, no. 3, pp. 1011–1037, May 2017, doi: 10.1007/s10694-016-0615-1.

[2] R. Van Coile, D. Hopkin, D. Lange, G. Jomaas, and L. Bisby, 'The Need for Hierarchies of Acceptance Criteria for Probabilistic Risk Assessments in Fire Engineering', *Fire Technol.*, vol. 55, no. 4, pp. 1111–1146, Jul. 2019, doi: 10.1007/s10694-018-0746-7.

[3] ISO, *ISO 834-1: Fire-resistance tests - Elements of building construction - Part 1: General requirements*, Geneva, Switzerland., 1999.

[4] T. Gernay and J. M. Franssen, 'A performance indicator for structures under natural fire', *Eng. Struct.*, vol. 100, pp. 94–103, Oct. 2015, doi: 10.1016/j.engstruct.2015.06.005.

[5] E. Annerel, L. Taerwe, B. Merci, D. Jansen, P. Bamonte, and R. Felicetti, 'Thermo-mechanical analysis of an underground car park structure exposed to fire', *Fire Saf. J.*, vol. 57, pp. 96–106, Apr. 2013, doi: 10.1016/j.firesaf.2012.07.006.

[6] T. Gernay *et al.*, *fib Bulletin 108. Performance-based fire design of concrete structures*. in fib Bulletins. fib. The International Federation for Structural Concrete, 2023. doi: 10.35789/fib.BULL.0108.

[7] U. Schneider, 'Verhalten von Beton bei hohen Temperaturen', Beuth Verlag, DE, DAfStb-Heft 337, 1982. Available: https://doi.org/10.2366/3702548

[8] U. Schneider, 'Behaviour of concrete under thermal steady-state and non-steady state conditions', *Fire Mater.*, vol. 1, no. 3, 1976, doi: 10.1002/fam.810010305.

[9] H. Weigler and R. Fischer, 'Influence of High Temperatures on Strength and Deformation of Concrete', *ACI Spec. Publ. SP-34*, Jan. 1972, doi: 10.14359/18082.

[10] M. Ghannam, 'Proposed models for concrete thermal expansion with different aggregate types and saturation conditions', *SN Appl. Sci.*, vol. 1, no. 5, pp. 1–13, 2019, doi: 10.1007/s42452-019-0452-1.

[11] Y. Anderberg and S. Thelandersson, 'Stress and deformation characteristics of concrete: experimental investigation and material behaviour model', *Univ. Lund Swed.*, vol. Bulletin 5, p. 86, 1976.

[12] R. Philleo, 'Some Physical Properties of Concrete at High Temperatures', *ACI J. Proc.*, vol. 54, no. 4, 1958, doi: 10.14359/11472.

[13] E. Annerel and L. Taerwe, 'Strain model for traditional and self-compacting concrete', *Fire Mater.*, 2013, doi: 10.1002/fam.2126.

[14] J.-M. Franssen, 'Thermal elongation of concrete during heating up to 700°C and cooling', 1993. [Online]. Available: https://hdl.handle.net/2268/531

[15] J.-M. Franssen and T. Gernay, ‘Modeling structures in fire with SAFIR® : theoretical background and capabilities’, *J. Struct. Fire Eng.*, vol. 8, no. 3, pp. 300–323, Aug. 2017, doi: 10.1108/JSFE-07-2016-0010.
[16] D. J. C. MacKay, ‘Bayesian Inference and Sampling Theory’, in *Information Theory, Inference, and Learning Algorithms*, Cambridge University Press, 2003.
[17] A. Gelman, J. B. Carlin, H. S. Stern, D. B. Dunson, A. Vehtari, and D. B. Rubin, *Bayesian data analysis*, Third edition. in Texts in statistical science series. Boca Raton London New York: CRC Press, Taylor and Francis Group, 2014.
[18] CEN, *EN 1992-1-2: Eurocode 2: Design of concrete structures - Part 1-2: General rules - Structural fire design*, Brussels, Belgium., 2004.
[19] J.-M. Franssen, ‘Contributions à la modélisation des incendies et de leurs effets sur les bâtiments’, Université de Liège, 1997. [Online]. Available: https://hdl.handle.net/2268/13644
[20] F. Put, B. Jovanović, E. Symoens, A. Lucherini, B. Merci, and R. Van Coile, ‘High-Intensity Fast-Response Electric Radiant Panel (HIFREP) to Impose Fire Equivalent Heat Fluxes on Building Elements with Enhanced Thermal Boundary Conditions Accuracy’, *Fire Technol.*, May 2025, doi: 10.1007/s10694-025-01758-2.
[21] Hukseflux Thermal Sensors, ‘User manual SBG01 - Water cooled heat flux sensor’. 2023.
[22] Insulcon N.V., ‘Insulfrax LTX Blanket’, Insulcon N.V., Technical datasheet 03032025/CD/jj, 2025.
[23] Keramab N.V., ‘Calcon Board 1000-SC’, Keramab N.V., Technical datasheet 16092014/BA/ka, Aug. 2012.
[24] J.-M. Franssen, ‘SAFIR: A Thermal and Structural Program for Modeling Structures Under Fire’, *Eng. J.*, vol. 42, no. 3, pp. 143–158, Sep. 2005, doi: 10.62913/engj.v42i3.856.
[25] N. Metropolis, A. W. Rosenbluth, M. N. Rosenbluth, A. H. Teller, and E. Teller, ‘Equation of State Calculations by Fast Computing Machines’, *J. Chem. Phys.*, vol. 21, no. 6, pp. 1087–1092, Jun. 1953, doi: 10.1063/1.1699114.
[26] W. K. Hastings, ‘Monte Carlo sampling methods using Markov chains and their applications’, *Biometrika*, vol. 57, no. 1, pp. 97–109, Apr. 1970, doi: 10.1093/biomet/57.1.97.
[27] B. Jovanović, R. Caspeele, E. Reynders, G. Lombaert, and R. Van Coile, ‘Bayesian Updating Methodology for the Post-fire Evaluation of the Maximum Temperature Profile Inside Concrete Elements’, *Fire Technol.*, vol. 60, no. 3, pp. 2155–2175, May 2024, doi: 10.1007/s10694-024-01564-2.
[28] E. T. Jaynes, ‘Information Theory and Statistical Mechanics’, *Phys. Rev.*, vol. 106, no. 4, pp. 620–630, May 1957, doi: 10.1103/PhysRev.106.620.
[29] T. M. Cover and J. A. Thomas, ‘Chapter 12: Maximum entropy’, in *Elements of information theory*, 2nd ed., Hoboken, N.J: Wiley-Interscience, 2006.
[30] P. J. Brockwell and R. A. Davis, *Introduction to Time Series and Forecasting*. in Springer Texts in Statistics. Cham: Springer International Publishing, 2016. doi: 10.1007/978-3-319-29854-2.
[31] J. D. Hamilton, *Time series analysis*. Princeton, N.J: Princeton University Press, 1994.
[32] G. E. P. Box, G. M. Jenkins, G. C. Reinsel, and G. M. Ljung, *Time series analysis: forecasting and control*, Fifth edition. in Wiley series in probability and statistics. Hoboken, New Jersey: John Wiley & Sons, Inc, 2016.

[33] J. C. Mindeguia, I. Hager, P. Pimienta, H. Carré, and C. La Borderie, 'Parametrical study of transient thermal strain of ordinary and high performance concrete', *Cem. Concr. Res.*, vol. 48, pp. 40–52, 2013, doi: 10.1016/j.cemconres.2013.02.004.